Vegetation and climate effects on soil production, chemical weathering, and physical erosion rates

Mirjam Schaller[1], Todd A. Ehlers[1]

[1]University of Tuebingen, Department of Geosciences, Schnarrenbergstrasse 94-96, 72076 Tuebingen, Germany

Correspondence to: Mirjam Schaller (mirjam.schaller@uni-tuebingen.de)

Abstract

Weathering of bedrock to produce regolith is essential for sustaining life on Earth and global biogeochemical cycles. The rate of this process is influenced not only by tectonics, but also by climate and biota. Here we investigate these interactions with new observations of soil production, chemical weathering, and physical erosion rates from the large climate and vegetation gradient of the Chilean Coastal Cordillera (26° to 38°S). These findings are compared to a global compilation of published data from similar settings. The four Chilean study areas span (from north to south): arid (Pan de Azúcar), semi-arid (Santa Gracia), mediterranean (La Campana), and temperate humid (Nahuelbuta) climate zones. We test the hypotheses that: 1) soil production as well as chemical weathering rates increase with increasing mean annual precipitation rates up to a limit, at which point a non-linear relationship is observable; 2) physical erosion rates stabilize as vegetation cover increases; and 3) the contribution of chemical weathering to total denudation is constant over the climate gradient.

We find observed soil production rates range from ~7 to 290 t/(km^2 yr) and are lowest in the sparsely vegetated and arid north, increase southward toward the vegetated mediterranean climate, and then decrease, or remain the same, further south in the temperate humid zone. This trend is discussed and compared with global data from similar settings underlain by granitic lithologies. Calculated chemical weathering rates range from zero in the arid north to a high value of 211 t/(km^2 yr) in the mediterranean zone. Chemical weathering rates are moderate in the semi-arid and temperate humid zones (~20 to 50 t/(km^2 yr)). Similarly, physical erosion rates are lowest in the arid zone (~11 t/(km^2 yr)) and highest in the mediterranean climate zone (~91 t/(km^2 yr)). Therefore, the total denudation rates indicate the same trend as the soil production rates. The contribution of chemical weathering to total denudation rates increases and then decreases with increasing mean annual precipitation from north to south. The observation that the calculated chemical weathering rates in the southernmost location, with the highest mean annual precipitation and the highest chemical index of alteration, are not the highest of all four study areas is found to be consistent with the global data analysis.

1 Introduction

Regolith forms through the weathering of rock near the Earth's surface and contains a mobile soil[1] that overlies an immobile saprolite (weathered bedrock) (e.g., Heimsath et al., 1997; Riebe and Granger, 2013). Denudation of the mobile soil layer results in the continual supply of weathered bedrock towards the surface and replenishes nutrients for biota. Soil production from weathered bedrock in a soil-mantled hillslope occurs through complex interactions between tectonics (which influences the slope of topography and therefore denudation), rock type, climate (specifically precipitation and temperature), and biota. All of these soil production processes are active over extended (millennial and greater) timescales (e.g., Mishra et al., 2019; Starke et al., 2020). Disentangling the interactions between tectonics, climate, and biota on soil production has proved challenging and has previously been approached in study areas with diverse geologic, climate, and vegetation histories through the determination of soil production rates (e.g., Dixon et al., 2009; Dixon and von Blanckenburg, 2012; Heimsath et al., 2012; Larsen et al., 2014). The term soil production rate (SPR) is used here as a general term for the production rate of bedrock into saprolite or soil. Studies investigating SPRs typically operate under the simplifying assumption of steady-state conditions. Under steady-state conditions, SPRs are considered equal to surface denudation rates, which include mass loss through chemical weathering and physical erosion in soil and saprolite (e.g., Dixon et al., 2009). With these concepts in mind, the goal of this study is the quantification of soil production, chemical weathering, and physical erosion rates across diverse climate and ecological gradients. These data, in combination with a global inventory are used to identify the contributions of biotic and abiotic processes to SPRs.

Previous studies have investigated SPRs, chemical weathering, and physical erosion in different geologic (and lithologic) settings. Here we highlight related work in granitic settings, which are also the focus of this study. Previous work by Riebe et al. (2001) investigated chemical weathering rates based on the combination of cosmogenic nuclides measured in river sediment and immobile element concentrations (e.g., Zr or Ti) measured in soil, saprolite, and bedrock. In this approach, the enrichment of immobile elements in soil and saprolite (relative to bedrock) was used to separate denudation rates into chemical weathering and physical erosion rates (see also Riebe and Granger, 2013). Applied on different geographic locations in granitic settings around the world, spanning over mean annual precipitation (MAP) rates of 220 to 4200 mm/yr and mean annual temperatures (MAT) of 2 to 25ºC, Riebe et al. (2004a) observed that the highest chemical weathering rates occur in areas with high denudation rates.

In addition to recognition that chemical weathering rates are correlated with total denudation rates, the importance of climate and vegetation on weathering rates has also been observed. For example, the influence of climate on SPRs and chemical weathering rates has been documented in altitudinal transects (e.g., Riebe et al, 2004b; Dixon et al., 2009; Ferrier et al., 2012). More specifically, a decrease in chemical weathering rates was observed with increasing altitude and was attributed to changes

[1] The terms regolith, soil, and saprolite used in this study follow the notation of Riebe and Granger (2013). This notation is not consistent with the one used in soil sciences (IUSS Working Group WRB, 2015) where the terms soil/regolith, pedolith, and saprolith would be used, respectively.

in both snow depth and vegetation cover (Riebe et al., 2004b). In a different location (Dixon et al., 2009), an altitudinal transect documented a peak in chemical weathering rates that correlated with physical erosion rates in middle elevation positions. Dixon et al. (2009) attributed this result to climate variations affecting vegetation along the transect. In contrast to the previous studies, chemical weathering rates from two transects collected below tree line elevation were observed to be insensitive to regolith temperature differences as well as regolith moisture (Ferrier et al., 2012). Ferrier et al. (2012) concluded that there was no significant change in weathering rates observed due to the lack of biotic changes along the transects. In addition, other studies have identified that the contribution of chemical weathering rates to total denudation rates appears to remain constant for different denudation rates despite changes in MAP (e.g., Riebe et al., 2004a; Larsen et al., 2014). Taken together, the previous work suggests a sensitivity of chemical weathering rates to precipitation, temperature, and vegetation cover (Riebe et al., 2004b; Dixon et al., 2009), but also an insensitivity to regolith temperatures and moisture with a (inferred) sensitivity to biotic changes (Ferrier et al., 2012). Thus, the previous studies contain conflicting results and highlight uncertainty in our current knowledge.

Building upon the previous work, Oeser et al. (2018) and Schaller et al., (2018) investigated four study areas located along the extreme climate and vegetation gradient of the Chilean Coastal Cordillera (26° – 38°S). Their work documented that the total denudation rates first increase from north to south and then decrease further south despite increasing MAP rates and vegetation cover (Oeser et al., 2018, Schaller et al., 2018). In these Chilean study areas, the contribution of chemical weathering to total denudation rates was variable and almost zero in the arid north, ~50% in the semi-arid and mediterranean settings, but appeared reduced, to potentially equal (to the mediterranean setting), in the temperate climate of the southernmost study area (e.g., Oeser et al., 2018). The results of Oeser et al., (2018) and Schaller et al., (2018) highlight that both climate and vegetation effect soil production, chemical weathering, and physical erosion rates, but that the relationship is likely non-linear. More specifically, their work suggests that there is a limit to the effects of vegetation and climate on soil production, chemical weathering, and physical erosion rates in heavily vegetated and wet settings (e.g., the temperate south of the Chilean Coastal Cordillera). In addition, a non-linear relationship between vegetation and denudation rates was also recently documented along the western Andean margin (Precordillera) of Peru and Chile in recent work by Starke et al. (2020).

In this study, we build upon the previous work in two ways. First, we present 11 new cosmogenic nuclide measurements collected from four study areas along ~1,300 km of the extreme climate and vegetation gradient of the slowly eroding Chilean Coastal Cordillera (Fig. 1). These samples come from new pedon locations not previously investigated by Schaller et al. (2018), but located along the same hillslopes and with major element measurements available from previous work by Oeser et al, (2018). Given the contrasting results of previous studies (e.g., Riebe et al., 2004b; Dixon et al., 2009; and Ferrier et al., 2012) our aim with these new samples was to verify if our previous observations (Oeser et al., 2018) of latitudinal trends in soil production, chemical weathering, and physical erosion rates are valid for pedons located in different (i.e., top- and toe-slope) hillslope positions than the previously investigated mid-slope positions in Oeser et al. (2018). Second, equipped with the new results from the Chilean transect, we extend our analysis globally to similar data sets collected from granitic hillslope settings. Together, these two approaches provide a holistic picture of if any non-linear relationship(s) in soil production,

chemical weathering, and physical erosion rates exist across different climate and vegetation settings. To address the previous two aims, our efforts are focused on evaluating three hypotheses. These include: 1) soil production as well as chemical weathering rates increase with increasing MAP rates up to a limit, at which point a non-linear relationship is observable. This hypothesis stems from the initial observations of Oeser et al. (2018) and may explain differences observed between some previous studies (e.g., Riebe et al., 2004b; Dixon et al., 2009; Ferrier et al., 2012); 2) physical erosion rates stabilize as vegetation cover increases. This hypothesis emerged from the seminal work of Langbein and Schumm (1958), but was drawn into question through work by Starke et al., (2020); and finally, 3) the contribution of chemical weathering to total denudation is constant over the climate gradient. Hypothesis 3 is supported by work of Riebe et al. (2004a) and Larsen et al. (2014), but not by Oeser et al., (2018). If this hypothesis is true, the proposed relationship should be evident from the extended Chilean transect data presented here. We note that throughout this manuscript, our calculation of chemical weathering and physical erosion rates follows the approach, notation, and methods described in Dixon et al. (2009) and makes use of the geochemical data reported by Oeser et al. (2018).

2 Chilean study areas

The four study areas are located in the Chilean Coastal Cordillera (~26° to 38° S, Fig. 1; Table S1) and span (from north to south) climate and biogeographic zones ranging from arid to humid. Each area contains primarily granitic lithologies (mostly granodiorite, tonalite, quartz diorite) and to a lesser degree gabbro in the Santa Gracia area (Oeser et al., 2018). The Coastal Cordillera lies along the west coast of Chile, where the neighboring plate boundary is similar along strike underneath the Coastal Cordillera due to subduction of the Nazca Plate. The study areas were selected to keep differences in lithology and tectonic setting to a minimum and to enhance the signal of variable climate and vegetation on denudation rates.

In the following, we present the primary characteristics of the Chilean study areas that contain pedons in both south- and north-facing slopes. In all the study areas, no signs of glaciation are reported in previous literature or our own field observations. One caveat worth discussion is that the data sets considered in this study are sensitive to different time scales. For example, cosmogenic nuclide-derived denudation rates typically integrate over timescales of ~10^2-10^6 years, whereas vegetation and climate change can occur over similar and much shorter timescales. The comparison of modern climate and vegetation metrics to cosmogenic nuclide-derived denudation rates sensitive to these different timescales can introduce uncertainty into any interpretation. However, recent work has quantified climate and vegetation changes in the four study areas since the Last Glacial Maximum (LGM) and up to the Pliocene (e.g., Mutz et al., 2018; Werner et al., 2018). While LGM climate was wetter and cooler, the climate and vegetation gradients present today also existed in the past (Starke et al., 2020; Mutz et al., 2018; Mutz and Ehlers, 2019), thereby diminishing concerns that modern climate and vegetation gradients are a poor representation of past conditions that cosmogenic nuclide-derived denudation rates may be sensitive to. With this potential complication in mind, we proceed with presenting the present-day characteristics of each study area. Numbers reported in sections 2.1 to 2.4 are from previous work by Bernhard et al. (2018), Oeser et al. (2018), Schmid et al., (2018), and Schaller et al. (2018). The

combined thickness of A- and B-horizons is considered as soil thickness (see Table S1 in Oeser et a., 2018). The reported clay content, pH, and bulk density are the pedon averages of each study area (see Table 3 in Bernhard et al., 2018). The chemical index of alteration (CIA; after Nesbitt and Young, 1982) for bedrocks is a study area average whereas the CIA for regolith is reported for specific horizons (for more details see Table S5 in Oeser et al., 2018). The cosmogenic nuclide-derived denudation rates are reported for south- and north-facing mid-slope positions (see Oeser et al., 2018 and Table S6 in there).

2.1 Pan de Azúcar

In the northernmost study area Pan de Azúcar (Fig. 1; Fig. S1) MAP and MAT are 8 mm/yr and 21.1 °C (Karger et al., 2017). The very sparse higher desert vegetation covers 2% of the land surface. The Regosol containing pedogenic gypsum has soil thicknesses of 20 to 25 cm. The regolith has a clay content of 13.8 ±3.9%, a bulk density of 1.3 ±0.1 g/cm^3, and a pH of 8.1 ±0.1. The average CIA in bedrock is 55 whereas the CIA in regolith horizons can be as low as 31 due to atmospheric input. Cosmogenic nuclide-derived denudation rates from south- and north-facing mid-slope positions are 11.0 ±0.7 and 8.2 ±0.5 t/(km^2 yr) and dominated by physical erosion whereas chemical weathering is insignificant.

2.2 Santa Gracia

In Santa Gracia (Fig. 1; Fig. S1), MAP and MAT are 97 mm/yr and 17.7 °C, respectively (Karger et al., 2017). The soil horizons of this Cambisol are 30 to 55 cm thick. The clay content of the regolith is 11.1 ±4.9%, the regolith bulk density is 1.5 ±0.0 g/cm^3, and the pH is 6.3 ±0.3. The average CIA in the bedrock is ~43, which is similar to other granitic lithologies (i.e., 45 to 55; Nesbitt and Young, 1982) but lower than all the other study areas (52 to 55). The CIA in regolith horizons ranges from 49 to 52, indicating regolith weathering. The cosmogenic nuclide-derived denudation rates in the south- and north-facing mid-slope positions are 22.4 ±1.5 and 15.9 ±0.9 t/(km^2 yr). Chemical weathering rates are comparable to physical erosion rates.

2.3 La Campana

A mediterranean dry forest grows in La Campana (Fig. 1; Fig. S1) where MAP and MAT are 307 mm/yr and 14.1 °C, respectively (Karger et al., 2017). This forest covers 84% of the land surface. The Cambisol contains 35 to 60 cm thick soil horizons and a clay content of 10.5 ±1.6%. The regolith bulk density is 1.3 ±0.2 g/cm^3 whereas the pH is 5.4 ±0.3. The average CIA of the bedrock is 52 whereas the CIA of regolith horizons ranges between 50 to 58. Values of the cosmogenic nuclide-derived denudation rates are 53.7 ±3.4 and 69.2 ±4.6 t/(km^2 yr) for the south- and north-facing mid-slope positions. Reported chemical weathering rates are comparable to physical erosion rates.

2.2 Nahuelbuta

In the southern most study area of Nahuelbuta (Fig. 1; Fig. S1), the MAP and MAT are 1,479 mm/yr and 6.1 °C (Karger et al., 2017), respectively. The area contains a temperate mixed broadleaved-coniferous forest. Vegetation cover is as high as 95%. The regolith type is an Umbrisol with soil horizons as thick as 60 to 90 cm and a clay content of 26.2 ±2.6% in the regolith. Regolith bulk density and pH are 0.8 ±0.1 g/cm^3 and 4.3 ±0.2, respectively. The average CIA of bedrock is 54, whereas values in regolith horizons are as high as 75, indicating substantial weathering. Cosmogenic nuclide-derived denudation rates are 47.5 ±3.0 and 17.7 ±1.1 t/(km^2 yr) in the south- and north-facing mid-slope positions. Chemical weathering rates are lower than physical erosion rates.

3 Material and methods

Soil production, chemical weathering, and physical erosion rates were determined for top-, mid-, and toe-slope positions in the south-facing slopes, whereas only the mid-slope is investigated for the north-facing slopes. Cosmogenic nuclide concentrations of saprolite from 8 mid-slope positions are from Schaller et al. (2018) whereas 11 new top- and toe-slope position samples are presented here. Material analyzed for ^{10}Be concentrations to calculate SPRs are collected from the top of the saprolite made accessible by pedon excavation (e.g., www.earthshape.net; Bernhard et al., 2018; Oeser et al., 2018). The top of saprolite is considered to be the first encounter of in situ weathered bedrock represented by the C-horizon. This sampling strategy is a common approach for calculation of soil production rates from cosmogenic nuclide measured in pedons (e.g., Dixon et al., 2009). Representative photographs of this horizon from the Chilean study areas are available in Oeser et al., (2018: Figures 3 to 6). In our study, the depths sampled in each pit are shown in Supplementary Material table S2. Saprolite material was crushed and sieved into a 0.25–1.0 mm fraction. Further cleaning of sample material and extraction of Be followed the methods as described in Schaller et al. (2018). For previous, and all but one new, sample locations the chemical weathering and physical erosion rates were calculated from the SPRs and major and trace element concentrations in soil, saprolite, and bedrock. Major and trace element concentrations used for the samples are from Oeser et al. (2018). To summarize, we combine 11 new, with 8 previously published, cosmogenic nuclide concentrations to present 19 newly calculated SPRs and 18 newly calculated chemical weathering and physical erosion rates.

3.1 Soil production rates

SPRs from Chilean soil-mantled hillslopes (Table S2) were calculated as follows: The in situ-produced ^{10}Be concentration of quartz contains information about the regolith or SPR (e.g., Heimsath et al., 1997). The nuclide concentration C (atoms/g$_{(qtz)}$) of the uppermost saprolite sample at the sample location is a function of:

$$C = \sum_1^3 \frac{P_n(h,\theta)}{(\lambda + \frac{SPR}{\Lambda_n})} \quad (1),$$

where P_n is the nuclide production rate (atoms/($g_{(qtz)}$ yr)) at sample depth h (cm) corrected for shielding Θ (unitless) by nucleonic, stopped muonic, and fast muonic production, respectively. No shielding by topography (less than 1%) and snow has been taken into account whereas shielding by vegetation of 2.3% and 7.3% have been used in La Campana and Nahuelbuta, respectively (Plug et al., 2007). The SPR is the soil production rate (g/(cm^2 yr)), λ is the decay constant (/yr), and Λ_n are the mean nucleonic, stopped muonic, and fast muonic attenuation lengths of 157, 1500, and 4320 g/cm^2, respectively (Braucher et al., 2011). The nucleonic, stopped muonic, and fast muonic production rates at sea level high latitude of 3.92, 0.012, and 0.039 atoms/($g_{(qtz)}$ yr) (Borchers et al., 2016) were scaled to the sample location based on Marrero et al. (2016).

3.2 Chemical weathering and physical erosion rates

The calculation of chemical weathering and physical erosion rates for the Chilean study areas follows the equations in Dixon et al. (2009). The sum of all mass loss D_{total} (t/(km^2 yr)) is given by:

$$D_{total} = SPR + W_{sap} = E_{soil} + W_{soil} + W_{sap} \quad (2),$$

where SPR is the known soil production rate (t/(km^2 yr)), W_{sap} is the chemical weathering rate for saprolite (t/(km^2 yr)), W_{soil} the chemical weathering rate for soil (t/(km^2 yr)), and E_{soil} is the physical erosion rate for soil (t/(km^2 yr)). Following Riebe et al. (2004a) and Dixon et al. (2009), W_{sap} can be expressed with the help of immobile elements in saprolite and bedrock as:

$$W_{sap} = SPR\left(\frac{Zr_{sap}}{Zr_{rock}} - 1\right) \quad (3),$$

where Zr_{sap} and Zr_{rock} are the concentration of Zr in saprolite and bedrock, respectively. In contrast, W_{soil} can be expressed by:

$$W_{soil} = SP_{soil}\left(1 - \frac{Zr_{sap}}{Zr_{soil}}\right) \quad (4),$$

where Zr_{soil} is the average Zr concentration for soil samples from the pedon. Similarly, Zr_{sap} is the average Zr concentration of the saprolite samples from the pedon. Zr_{rock} is based on the average of all bedrock samples collected in one specific study area (see Table S3 based on Oeser et al., 2018). The chemical depletion fraction CDF_{total} is determined by the fraction of the total chemical weathering rate W_{total} (as the sum of W_{soil} and W_{sap}) and the total denudation rate D_{total} (Tables S4 and S5). As all results presented below are based on the notation of Dixon et al. (2009), the total denudation rates include the contribution of weathering in the saprolite. We note that this is in contrast to the total denudation rates presented in Oeser et al. (2018) which do not account for weathering in the saprolite and are considered as minimum denudation rate estimates.

3.3 Global data compilation, correlation, and model simulations

The hypotheses addressed in this study relate to the relationships between soil production, chemical weathering, physical erosion, and factors such as precipitation, slope, and vegetation cover. To evaluate these hypotheses, we present an analysis for both the new Chilean transect data and also a global compilation of previously published data from similar granitic sample locations as the Chilean data. More specifically, SPRs from the Chilean study areas were compared to previously published SPRs derived from granitic (Table S6) and non-granitic (Table S7) soil-mantled hillslopes from around the world. For both approaches (Chilean and global) we conduct our analysis in two ways.

First, we conduct a linear Pearson correlation analysis between relevant parameters to identify statistically significant relationships. These are presented in Table S8 with the corresponding Pearson R and P values for significance. For the globally distributed granitic sample locations, a range of topographic, climate, and vegetation parameters were compiled (see Supplemental text 1 for details and data sets used). These SPRs and parameters were also analyzed with a Pearson linear correlation analysis (Table S8). The MAP, MAT, leaf area index LAI, and SPRs at sample locations in the global compilation were also compared to available model predictions (for details see Supplementary Material S2). In addition, chemical weathering and physical erosion rates determined in granitic soil-mantled hillslopes around the world were compiled. The previous climate and vegetation parameters were compared to chemical weathering and physical erosion rates (Table S10) also using a Pearson correlation analysis (Table S8, S9).

In addition (second), we compare observations to previously proposed theoretical/modelling approaches. In particular, we compare results to the models of: (1) Norton et al. (2014) which predicts the maximum SPR for different MAP and MAT; (2) a modified version of the Norton et al. (2014) approach that also accounts for the effect of variable soil thickness with changing MAP on SPR; and (3) Pelak et al. (2016) who predicted SPR as a function of biomass density and soil depth. The details of each approach and governing equations are provided in Supplementary Material S2. Finally, for completeness we also compared results (presented in Supplemental Material S2) to the effective energy and mass transfer (EEMT) approach of Pelletier and Rasmussen (2009). This later approach accounts for SPR changes as a function of MAT and MAP taking into account the influence of biotic control on EEMT. However, the results are not presented in the main text because this model did not provide a satisfactory fit to the observations. Nevertheless, we include it in the Supplementary Material for the curious reader.

4 Results

In this section, results for soil production, chemical weathering, and physical erosion rates are presented for the new and previously published cosmogenic nuclide concentrations from the Chilean study areas (Fig., 2; Tables S2, S4, and S5). Results are given for each study area starting in the arid north and progressing to the south. The total denudation rates (D_{total}) presented below are the composite of the total chemical weathering rate (W_{total}) and the physical erosion rate (E_{soil}) and based on the calculated SPRs and the Zr concentrations in rock, saprolite, and soil (Table S3). Because the observations presented in our global compilation were previously published (see references in Tables S6 and S8), we do not present the compilation in this section but rather in section 5 (Discussion) where it is integrated and discussed in the context of our Chilean observations. In addition, correlations of SPRs as well as chemical weathering and physical erosion rates with parameters are also shown in section 5.

4. 1 Pan de Azúcar

The in situ-produced ^{10}Be concentrations in quartz range from (2.58 ±0.08) 10^5 atoms/$g_{(qtz)}$ to (5.08 ±0.16) 10^5 atoms/$g_{(qtz)}$ (Table S2). The south-facing slope of Pan de Azúcar has SPRs that increase from 7.7 ±0.5 t/(km^2 yr) in the top-slope position to 16.8 ±1.0 t/(km^2 yr) in the toe-slope (Fig. 2A; Table S2). The north-facing mid-slope position has a lower SPR than the south-facing mid-slope position. The average Zr concentration of bedrock in Pan de Azúcar is 206 ±8 ppm, whereas Zr concentrations in soil and saprolite are between 184 ±14 and 272 ±75 ppm (Table S3). The averaged Zr_{soil}/Zr_{rock} ratio in Pan de Azúcar is 1.07 ±0.09 (Table S4) indicating no enrichment of the immobile element Zr from rock to soil. Chemical weathering rates are low <1.7 ±0.8 t/(km^2 yr); Fig. 2B; Table S4) and with an average value of 0.3 ±0.3 t/(km^2 yr). The average total denudation rate of 11.0 ±0.24 t/(km^2 yr) is dominated by the physical erosion rate with an average value for the study location of 10.7 ±2.6 t/(km^2 yr). This results in an average CDF_{total} of 0.05 ±0.08 (Table S5).

4. 2 Santa Gracia

In Santa Gracia, ^{10}Be concentrations in quartz range from (1.75 ±0.06) 10^5 atoms/$g_{(qtz)}$ and (4.19 ±0.23) 10^5 atoms/$g_{(qtz)}$ (Table S2). In the south-facing slope of Santa Gracia, where six samples were collected from top- to toe-slope positions (Tables S1 and S2), SPRs generally increase downslope from 17.8 ±1.3 to 28.0 ±1.7 t/(km^2 yr). The SPR in the north-facing mid-slope position is lower than the equivalent mid-slope position in the south-facing slope (Fig. 2A; Table S2). The Zr_{soil}/Zr_{rock} ratios are around 2 but subject to a large uncertainty due to inhomogeneity in the Zr_{rock} concentration (Table S3). Nevertheless, the averaged ratio of Zr_{soil}/Zr_{rock} is 2.10 ±0.08 indicating enrichment of the immobile element Zr from rock to soil. An estimated 80% of the weathering is located in the saprolite (Table S4). Total chemical weathering rates range from 11.0 ±5.4 t/(km^2 yr) to 30.4 ±16.0 t/(km^2 yr) (Fig. 2B). Higher chemical weathering rates are calculated for weathering in saprolite than in soil (Fig. S2; Table S4). Total chemical weathering and physical erosion rates contribute equally to the total denudation rate (Table S5). This is reflected in the average CDF_{total} of 0.52 ±0.02.

4. 3 La Campana

In situ-produced ^{10}Be concentrations in La Campana range from (0.22 ±0.01) 10^5 atoms/$g_{(qtz)}$ to (1.61 ±0.06) 10^5 atoms/$g_{(qtz)}$ (Table S2). In La Campana the SPRs in the south-facing slope increase from top- to toe-slope with values of 42.1 ±2.6 to 290.5 ±24.0 t/(km^2 yr)) (Table S2). The SPR in the north-facing mid-slope position is slightly higher than the rate in the equivalent south-facing position (Fig. 2A; Table S2). Zirconium concentrations from rock to soil increase in La Campana (Table S3). The chemical weathering rates in La Campana range from 20.2 ±2.6 t/(km^2 yr) to 210.5 ±34.3 t/(km^2 yr). About 60% of the chemical weathering occurs in the saprolite. The average total chemical weathering rate in La Campana of 95.0 ±44.7 t/(km^2 yr) is affected by a large standard error of the mean. This large error arises from the exceptionally high SPR of

sample LCPED30 likely related to the high topographic slope of 35°. The average CDF_{total} is 0.49 ±0.07 indicating that half of the total denudation is due to chemical weathering (Table S5).

4. 4 Nahuelbuta

^{10}Be concentrations in quartz range from (1.24 ±0.05) 10^5 atoms/$g_{(qtz)}$ to (3.83 ±0.13) 10^5 atoms/$g_{(qtz)}$ (Table S2). The SPRs from the south-facing slope in Nahuelbuta are within error, but increase slightly downslope from 57.7 ±3.5 to 68.6 ±4.2 t/(km^2 yr) (Table S2). The SPR in the mid-slope position of the north-facing slope is much lower than the rate from the mid-slope position in the south-facing slope (Fig. 2A; Table S2). The increase of zirconium from rock to soil is less pronounced in Nahuelbuta than in Santa Gracia or La Campana (Averaged Zr_{soil}/Zr_{rock} ratio of 1.39 ±0.12; Tables S3 and S4). Chemical weathering rates indicate a wide range between 4.4 ±15.5 t/(km^2 yr) to 31.3 ±5.1 t/(km^2 yr). Physical erosion rates vary between 20.0 ±1.2 t/(km^2 yr) and 55.1 ±3.5 t/(km^2 yr). The average CDF_{total} of 0.27 ±0.06 indicates that the physical erosion rate is higher than the chemical weathering rate (Tables S4 and S5).

In summary, SPRs generally increase from Pan de Azúcar to La Campana and are lower, or possibly equal, again in Nahuelbuta (Fig. 2A). From north to south, the same trend is observed in the chemical weathering rates (Fig. 2B) as well as in the physical erosion rates (Fig. 2C). Therefore, the total denudation rate combining chemical weathering and physical erosion rates increases from Pan de Azúcar to La Campana and seems to decreases in Nahuelbuta to a slightly higher value than in Santa Gracia (Fig. 2D). The CDF_{total} values and the contribution of W_{total} to D_{total} are almost zero in Pan de Azúcar. In Santa Gracia and La Campana they are about equal (~0.5), and then they are reduced in Nahuelbuta (~0.3; Table S5). Nevertheless, W_{total} and D_{total} of all samples from the four study areas correlate very well ($R^2 = 0.96$) with a slope of 0.50 (Fig. S3A).

5 Discussion

In the following sections, the soil production, chemical weathering, and physical erosion rates calculated for the Chilean study areas are discussed and compared to the global compilation. Whereas section 5.1 addresses SPRs, section 5.2 discusses findings and problems observed with chemical weathering and physical erosion rates.

5.1 Soil production rates

In this section SPRs from the Chilean Coastal Cordillera are compared to a global data compilation of SPRs from granitic soil-mantled hillslopes in the light of MAP of the sample locations. The global data compilation from granitic lithologies is investigated for correlations of SPRs with topography, climate, and vegetation (leaf area index, LAI) metrics. Lastly, the SPRs are compared to model predicted variations in SPRs for different climate and vegetation settings.

5.1.1 Comparison of global SPR compilation based on MAP

The SPRs in the Chilean Coastal Cordillera increase from north to south from Pan de Azúcar to La Campana and are slightly lower, or possibly equal, again in Nahuelbuta (Fig. 2A). Comparison of MAP to the Chilean and global compilation of SPRs from soil-mantled hillslopes on granitic lithologies highlights several commonalities (Fig. 3A, Table S6). The maximum in SPRs (~900 t/(km^2 yr)) occurs at MAP values between ~500 to 600 mm/yr. After this maximum, SPRs generally decrease with increasing MAP with the exception of two SPRs from a mountain crest with zero slope that form a second maximum (red symbols, Fig. 3A, from the Jalisco Highlands; Riebe et al., 2004a). The maximum in SPRs is dominated by locations with high slopes (>30°; green symbols, Fig. 3A) from the tectonically active San Gabriel Mountains (Heimsath et al., 2012). The findings of high SPRs with steep slopes are consistent with previous work (e.g., Binnie et al., 2007). The second maximum (Jalisco Highlands) is the result of highest SPRs reported from hillslopes with little or no soil (e.g., see findings of Heimsath et al., 1997). However, due to the reported low slope at a mountain crest the two data points from the Jalisco Highlands (Riebe et al., 2004a) are excluded from further analysis. Furthermore, the highest SPRs from samples with slopes >30° (Fig. 3A) agree well with the maximum SPRs for bare rock predicted from the 'maximum SPR model' of Norton et al. (2014; black line Fig. 3A, see also Supplementary Material S2 for summary of model equations). This model predicts a linear increase in SPRs with increasing MAP. A purely linear relationship between SPRs and MAP is not evident for either the Chilean or global data sets for MAP > ~600 mm/yr, or for locations with slopes <30° (Fig. 3A). We also note that a similar increase and then decrease in SPRs with increasing MAP is observed for non-granitic soil-mantled hillslopes (Fig. 3B). However, the maximum SPRs in these settings are not only higher than in granitic lithologies but also reached at a higher MAP (~3,000 mm/yr; see also discussion section 5.3). This discrepancy between the trend in SPR with MAP for granitic versus non-granitic catchments is perplexing, but is most easily explained by previous work that highlights the importance of lithology and rock strength variations when interpreting SPRs (e.g., Heimsath and Whipple, 2019).

The previously described trend of an increase and then decrease in SPR with increasing MAP is in contrast with the increase of SPRs predicted from the maximum SPRs for bare rock predicted with the model of Norton et al. (2014). The difference between observation and prediction could suggest that additional factors other than MAP influence the relationship. The observed decrease in SPR at MAP >600 mm/yr (Fig. 3A) could, for example, be attributed to other climate and vegetation effects on SPR and soil thickness (e.g., Langbein and Schumm, 1958; Amundson et al., 2015; Richardson et al., 2019; Mishra et al., 2019; Starke et al., 2020). We note that the relationship between SPR and MAP identified here for Chile, and also present in the global compilation, are not a new result (e.g., Mishra et al., 2019), but have been obfuscated in previous studies by nature of the data being plotted in log-log (e.g., Fig. 3C) rather than linear plots (e.g., Fig. 3A and 3B and all other plots of this study). In the following, we investigate the non-linear effect of climate and vegetation on SPRs (for granitic soil-mantled hillslopes only) with respect to different location specific parameters (e.g., MAT, LAI, slope, soil thickness).

5.1.2 Correlation of SPRs with topography, climate, and vegetation parameters

As expected from the previous section, the SPRs of granitic soil-mantled hillslopes and MAP are only weakly (inversely) correlated ($R = -0.16$; $p < 0.05$; Table S8). The best, but still weak, linear correlation of SPRs is achieved with local slopes (DEM GTOPO30; $R = 0.37$; $p < 0.05$; Table S8). Other parameters weakly correlating with SPRs are the mean altitude and MAT at the sample location. Remaining parameters investigated correlate even more weakly with SPRs than the previously mentioned slopes, mean altitude, and MAT correlations. In summary, based on the above linear correlation analysis, there is little evidence for any one parameter exerting a linear control on SPR. Given this, in the following the non-linear relationship between SPRs and three parameters (MAP, MAT, and LAI) are investigated in more detail before we compare these relationships to different proposed models for SPR (Fig. 4). As previously mentioned, SPRs increase with increasing MAP and then decrease. However, hillslopes with slopes >30° clearly document the highest SPRs (e.g., green symbols, Fig. 4) and SPRs increase with increasing slopes (Fig. S4). Therefore, we group SPRs into slope bins and apply polynomial fits to the different slope bins to qualitatively help guide the readers eye for the trend in the data.

We find that the maximum in the peak of the SPRs shifts to higher MAP values with decreasing slopes (Fig. 4A), but regardless of the slope the same general trend in the data is evident whereby SPRs initially increase, and then decrease towards higher MAP. The relationship between SPR and MAT is less clear (Fig. 4B) aside from that SPRs generally decrease with decreasing slopes. Furthermore, there is a shift from a peak in SPRs at ~10ºC for slopes of >30° (green line in Fig. 4B) to maximum values in SPRs occurring at low temperatures for slopes <20° (orange and red lines, Fig. 4B). In contrast, we find SPRs increase with increasing LAI to a maximum value of LAI = ~2.2 m^2/m^2 irrespective of slope (Fig. 4C). Furthermore, low SPRs can be found in landscapes with either thin soils and low MAP or thick soils and high MAP (Fig. S5). Whereas the former are landscapes with low LAI, the latter are governed by high LAI. For example, in landscapes subjected to a dry climate (e.g., Pan de Azúcar Chilean site), thin soils with little vegetation cause reduced SPR due to a combination of diminished abiotic and biotic weathering processes. Reduced SPRs are also observed in landscapes with a humid climate (e.g., Nahuelbuta Chilean site) with thick soils, and abundant vegetation. As SPR depends on both chemical weathering and physical erosion a more detailed discussion is presented concerning patterns in chemical weathering and physical erosion rates.

5.1.3 Comparison of predicted climate and vegetation effects on SPRs

Previous observations of SPRs, climate, and vegetation have motivated different approaches to identify the functional relationship between these parameters. These studies stem from the empirically derived relationship proposed by Heimsath et al. (1997). Here we highlight three previous approaches (e.g., Fig. 5 and S6) aimed at quantifying the effects of MAP, MAT, and in some cases LAI, on SPRs (see Supplementary Material S2 for equations used). An overview of the approaches considered are as follows. First, Norton et al. (2014) developed an empirical soil production function to determine maximum SPRs based on MAP, MAT, and variable depth of soil cover (Fig. 5A and B). Second, Pelletier and Rasmussen (2009) used the "effective energy and mass transfer" (EEMT) approach of Rasmussen and Tabor (2007) to calculate SPRs (Fig. S6). Biotic

controls are included in EEMT through the influence of MAP and MAT on biota. Finally (third), Pelak et al. (2016) developed a production rate function assuming the abiotic production rate is constant, and the biotic effects are calculated based on present-day soil depth and vegetation biomass (Fig. 5C). The previous studies suggest markedly different functional relationships between MAP, MAT, vegetation, and SPRs, thereby highlighting uncertainty in our current knowledge.

General trends in the controls on SPRs are, however, visible from observations. Maximum SPRs (under a constant average MAT of 14°C) are predicted to increase rapidly with increasing MAP to high values (Fig. 5A, black bold line). The maximum SPRs of Norton et al. (2014) explain the observed highest rates, but fail to capture the observed decrease in SPRs with increasing MAP (at MAP > ~600 mm/yr). Furthermore, the Norton et al. model predicts that if soil depths are thicker than predicted maximum SPRs decrease (Fig. 5A, black stippled lines). However, the previously described approach of Norton et al. (2014) does not account for increases in soil depth that are observed with increasing precipitation and vegetation cover (e.g., Rasmussen and Tabor, 2007; Pelak et al., 2016). To explore the combined effects of variable soil depth with MAP (and hence vegetation cover) on SPRs we modified the approach of Norton et al. (2014) (see Supplementary Material S2) to account for increasing soil depth with increasing MAP (Fig. 5A; blue curve). Using this modified approach, the SPRs reach a maximum around 1,100 mm/yr MAP and then decrease with higher MAP. This modification to the approach of Norton et al., (2014) results in a predicted relationship more similar to global observations whereby SPRs initially increase, reach a maximum value, and then decrease as MAP increases. Although the blue curve in Fig. 5A does not provide a good fit to observations (in part because each sample location has a different MAT), we note that the general trend in the model predictions and data are more closely matched, thereby highlighting the potential importance of considering soil depth variations in this type of analysis. The relationship between MAT and SPR is less clear (Fig. 5B). Here, the predicted maximum SPRs using the approach of Norton et al., (2014) are shown for different MAT (Fig. 5B), assuming no soil depth (black line) or stable soil depth (stippled lines). Comparison between the predicted and observed SPR shows a general disagreement between model predictions and observations using this approach.

The influences of MAP and MAT on SPR are often conceptualized as the main contributors to abiotic weathering. However, variations in MAP and MAT are a controlling factor in vegetation type and amount, which potentially influence biotic weathering and SPRs through their demand for nutrients. Support for vegetation influencing SPRs comes from the work of Pelak et al. (2016) (Fig. 5C, see Supplementary Material S2 for equations). In their approach, SPRs are calculated as a function of biomass, which we represent with increasing LAI for comparison to our observations. This approach predicts an initial increase in SPRs with increasing LAI. The LAI value at which the maximum in SPRs occurs depends on the ratio of the vegetation growth rate (r) over the vegetation turnover time (m) (black curves Fig. 5C, see also Supplementary Material). The predicted increase then decrease in SPR shown in figure 5C is similar to the globally observed increase then decrease in SPRs with LAI.

In summary, based on the previous considerations, we find that global variations in observed SPRs can be explained by variations in slopes, MAP, soil depth, and vegetation cover worldwide (Fig. 5). Our interpretation is based on diverse factors that influence vegetation cover and both the biotic and abiotic 'engines' contributing to soil production. In addition to MAP

and soil depth, we find that SPRs vary with topographic slope (Fig. 4A and S4, see also Heimsath et al.; 1997) and MAT. Although available data do not allow a comparison of SPRs to rates of tectonic uplift, variations in tectonic uplift rates in the global compilation are indirectly represented by variations in hillslope angle. Given this, the relationships between SPR and MAP (e.g., Fig. 3) for diverse slopes suggests that regardless of the rate of tectonic uplift (likely manifested in different slopes) the trends in SPR document here exist. More specifically, although high-slope settings produce the highest SPRs, the trends in MAP and vegetation cause an increase and then decrease in SPRs as MAP or LAI increase regardless of the hillslope angle (compare green and red lines, Fig. 4A, C).

5. 2 Chemical weathering and physical erosion rates

In this section chemical weathering and physical erosion rates, and CDFs for the Chilean Coastal Cordillera are discussed. In addition, CDFs of this study are compared to the CIA available for the climate and vegetation gradient of the Chilean Coastal Cordillera (Fig. 6). The Chilean data set is then compared to a global data compilation of soil-mantled hillslopes on granitic lithologies.

5.2.1 Chilean data and relationships between climate, vegetation, and weathering

Chemical weathering and physical erosion rates as well as CDFs are subject to large uncertainties due to incorporation of Zr concentrations for calculation. Zr concentrations in bedrock, saprolite, and soil can be highly variable and affect the calculation of weathering rates. Furthermore, available bedrock outcrops for sampling at neighboring locations may not be representative of the material the soil and saprolite formed from, as observed in our Santa Gracia Chilean study area (e.g., Fig. 9 and 10b in Oeser et al., 2018). Whereas this complication does not influence the calculation of W_{soil} or E_{soil} (and hence SPR), W_{sap} and D_{total} are affected by inaccuracies in the Zr concentration used. In the cases where the Zr concentration of the average bedrock is lower than the Zr concentrations in soil and saprolite (Table S3), the calculated W_{sap} and hence D_{total} are reasonable.
In contrast, if the Zr concentration in the saprolite is lower than the concentration in the bedrock then W_{sap} and hence D_{total} need to be interpreted with care. The calculated fraction of weathering in saprolite is negative and D_{total} is underestimated. The too low concentrations of Zr and also Ti in the saprolite are not consistent with the assumption that soil production occurs from bedrock to saprolite and then soil (Table S3). Difficulties may also arise from aeolian and pedogenic input as, for instance, in the arid Pan de Azúcar study area, where pedogenic gypsum in the soil is reported (Bernhard et al., 2018). However, this pedogenic input only marginally affects the calculation of SPRs and D_{total}. Even though the calculation of chemical weathering and physical erosion rates are affected by large uncertainties some insights may be gained. For example, average CDF_{total} values of 0.05 ±0.08 to 0.52 ±0.02 reported for the four study areas (Table S5) indicate that where chemical weathering occurs, it may contribute up to 50% of the total denudation rate. The low CDF_{total} value of Pan de Azúcar can be explained by the absence of chemical weathering agents (e.g., carbonic acid produced from plant litter) and high pH. However, the CDF_{total} value of 0.27 ±0.06 reported from Nahuelbuta and hence the lower W_{total} in Nahuelbuta than La Campana to the north requires further consideration.

The low CDF_{total} in Nahuelbuta cannot be explained by the lack of a weathering agent nor by the influence of temperature on chemical weathering and physical erosion. For example, the wetter climate in Nahuelbuta than La Campana or Santa Gracia would suggest a high W_{total} in Nahuelbuta. This is shown by calculation of the silica fluxes in the four study areas based on equation 1 and values in Fig. 7 from Dixon et al. (2009). The calculated silica fluxes in Pan de Azúcar, Santa Gracia, La Campana, and Nahuelbuta are 14, 136, 316, and 746 mol/(ha yr), respectively. These calculations indicate that the silica flux under the climate conditions in Nahuelbuta should be double the fluxes calculated for La Campana. This is clearly not reflected in the W_{total} values reported in this study. High weathering rates in Nahuelbuta are also expected due to the reported CIA for soils of 75 in Nahuelbuta, which are higher than CIA in soils of the other study areas (Oeser et al., 2018).

Two explanations for the low values of W_{total} in Nahuelbuta could be based on the assumptions made for the calculations. First, in Nahuelbuta, low bulk densities in regolith (0.8 ±0.1 g/cm^3) and high clay contents (>25 %) are observed (Bernhard et al., 2018). These regolith properties could indicate volcanic input. The volcanic input, in turn, could dilute the Zr concentration in soil and result in an underestimate of W_{soil}. However, the chemical composition of the regolith and the pedogenic oxide content reveal no major volcanic influence in Nahuelbuta (Oeser et al., 2018).

A second explanation for the low values of W_{total} in Nahuelbuta could be a mobile behavior of the immobile elements (e.g., Yoo et al., 2007). Intense weathering of primary minerals should result in high Zr enrichment in soil unless Zr is mobile. The observation that the clay fraction in granitic regoliths is depleted in Zr (Taboada et al., 2006) supports the possibility that during weathering of primary to secondary minerals Zr is lost. The observation that the Zr concentration in regolith decreases with a decreasing Si to Al ratio in combination with the observation that secondary minerals have lower ratios of Si to Al than primary minerals (Yoo et al., 2007), further supports the possibility of Zr loss during weathering. Due to this possible Zr loss in regolith, the calculated W_{soil} is a minimum value which may underestimate W_{total} and overestimate E_{soil}. Unfortunately, based on the available information, it is not clear if insulation by thick soils (Burke et al., 2007) and/or Zr loss by intense chemical weathering (Yoo et al., 2007) could cause low values of W_{soil} and a low CDF_{total} in Nahuelbuta. Recalculation of chemical weathering and physical erosion rates based on the assumption of an expected CDF_{total} of 0.5 in Nahuelbuta does not lead to higher W_{total} in Nahuelbuta than La Campana. After recalculation, the approximated averaged W_{total} is ~30 t/(km^2 yr) instead of 19.6 ±7.8 t/(km^2 yr). With recalculation W_{sap} does not change but W_{soil} increases (from 9.10 ±8.23 t/(km^2 yr) to ~19 /(km^2 yr)) and E_{soil} decreases (from 39.4 ±10.3 t/(km^2 yr) to ~30 t/(km^2 yr)). Whereas W_{total} after correction is still higher in La Campana than in Nahuelbuta, W_{soil} is comparable. The recalculated E_{soil} of Nahuelbuta is still lower than the rate in La Campana. The decrease in physical erosion rate may result from stabilizing effects of plants. Total denudation rates D_{total}, which did not change due to the recalculation, increase from Pan de Azúcar to La Campana and decrease slightly, or possible stay the same in Nahuelbuta.

A third explanation for lower weathering rates in Nahuelbuta than La Campana could also be the effect of microbial activity (e.g., Buss et al., 2005; Eilers et al., 2012). Precipitation, temperature, and pH all affect microbial abundance (e.g., Fierer and Jackson, 2006; Bahram et al., 2018; Tan et al., 2020). For instance, microbial abundance increases and decreases along a tropical elevation-climate gradient where MAP increases and MAT decreases with increasing elevation (Peay et al., 2017). A

comparable increase in MAP and decrease in MAT is observed in the Chilean Coastal Cordillera, which may explain the decreasing pH values from north to south and the lower bacterial abundance in Nahuelbuta than La Campana (Bernhard et al., 2018; Oeser et al., 2018). In order to investigate if the above made hypotheses are valid in our study area, we proceed to compare data form this study with a global data compilation from granitic soil-mantled hillslopes.

5.2.2 Comparison to global data compilation

Similar to the Chilean Coastal Cordillera, the global data compilation also shows an increase and then decrease in the chemical weathering, physical erosion, and total denudation rates with increasing MAP (Fig. 6). In general, values of the CDF are around 0.4 to 0.6 in the global data compilation (Fig. 6 and S3B), and suggest similar physical erosion and chemical weathering rates as observed in some other studies (e.g., Riebe et al., 2001; Dixon et al., 2009; Granger and Riebe, 2014). However, values below and above 0.4 to 0.6 are also observed (Fig. 6). CDF values above 0.6 indicating extreme weathering rates are rare. CDF values corrected for the chemical erosion factor after Riebe and Granger (2013) from Puerto Rico and McNabb Track in New Zealand are higher than 0.6 (Table S9). More often, CDF values are lower than 0.4 and may even be close to zero indicating that chemical weathering is not operative or occurs only at low rates (e.g., Riebe et al., 2004a; Norton and von Blanckenburg, 2010; Ferrier et al., 2012). CDF values below 0.4 are reported from dry and hot places with low vegetation where water as a weathering agent is rare (e.g., Pan de Azúcar, this study). Other settings with low CDF values were previously encountered in cold regions with frost cracking and/or snow (e.g., Idaho Batholith, Ferrier et al., 2012; Switzerland, Norton and von Blanckenburg, 2010). Chemical weathering in cold regions might be low due to low temperatures, which in turn enable frost cracking and snow to increase physical erosion rates and diminish CDFs (Table S9). However, not only do climate and vegetation influence values of CDFs, but so does topography. For example, low CDFs are reported from Point Reyes in California by Burke et al. (2007). This study area is underlain by a granodioritic lithology and located in a mediterranean climate with 800 mm/yr of precipitation (Heimsath et al., 2005). The vegetation cover is grassland, shrubs, and trees, which host pocket gophers. CIA values of 59 for bedrock and 63 to 91 for soils (average 81) are reported. CDF values range from 0.06 to 0.75 with an average of 0.26. Average CDF values of thin soils (<60 cm) in divergent slope positions are 0.51, whereas thick soils (>60 cm) in a divergent position and soils in convergent positions indicate an average value of 0.13. Burke et al. (2007) concluded that thick soils act as a buffer against intense chemical weathering and inhibit high chemical weathering rates.

In summary, the decrease of CDFs with increasing MAP could be explained by reduced chemical weathering of saprolite due to buffering by thick soils (e.g., Burke et al., 2007). The protective nature of thick soils may distance vegetation from “fresh” nutrients in bedrock thereby leading to nutrient recycling (e.g., Oeser and von Blanckenburg, 2020; Koester et al., 2020) rather than nutrient acquisition from unweathered bedrock. This finding is consistent with previous work that has identified a decrease in chemical weathering rates with increased soil thickness as well as a ‘speed limit’ to chemical weathering rates (e.g., Dixon and von Blanckenburg, 2012). In essence, dense vegetation could be functioning as a ‘biotic break’ on soil production and weathering.

5.3 Study caveats and challenges

There are several caveats associated with this study that could influence the interpretations presented. In this study, we have made an effort to account for as many factors as possible. Nevertheless, due to our disciplines continually evolving understanding of how climate, tectonics, and the biosphere interact at the Earth's surface, there inevitably remain challenges to our approach that could be considered in future studies. We first discuss these potential caveats in terms of other processes that could be important, but that are currently difficult to quantify. Furthermore, (second) we discuss some potential methodological considerations.

First, the chemical, biologic, physical weathering and erosion processes addressed in this study are sensitive to a variety of factors that are either unknown, or known and difficult to quantify with existing data. For example, previous work by Oeser et al. (2018) documented mineralogical and geochemical differences between lithologies of the Chilean study areas. While we have restricted our analysis (as much as possible) to "granitic lithologies" there are still compositional differences between the different types of granites present. The mineralogical differences between different granitic rocks could influence the rates of chemical weathering. This concern also applies to our global compilation of granitic sample locations. Although this study filtered study areas by rock type, significant work remains to be done in quantifying chemical weathering rates within different lithologies as such as types of granite (e.g., Lebedeva and Brantley., 2020). In addition, the Chilean and global datasets contain geographic variations in rates of rock uplift. Our approach here was to identify if chemical weathering and physical erosion rates correlate with topographic slope, which is often considered a proxy for rock uplift rate. This connection is made as high slopes commonly occur in areas with high rates of rock uplift and lower slopes occur in more tectonically quiescent settings. While this approach is often used for a qualitative comparison, it does not provide a direct quantitative comparison between rates of tectonic activity and weathering and erosion processes. To address this concern, a global compilation of rock uplift rates, and other potentially related factors such as fracture density, would be needed for the correlation analysis. Unfortunately, these data sets do not exist. Finally, this study evaluated not only how present-day climatology (precipitation and temperature) compare to observed SPR and weathering rates, but also how these results would differ based on available paleo-precipitation and temperature estimates for the Middle Holocene and LGM (Table S6). This approach is useful for evaluating if a legacy of past climate conditions correlates with observed weathering and erosion processes (which it did not in our case). A similar conclusion was reached for the western Andean margin (Precordillera) of Peru and Chile in work by Starke et al. (2020). However, our approach does not address the full range of potentially relevant paleo-conditions. For example, while changes in LGM or Mid Holocene precipitation and temperatures exist, their effect on paleo-solute fluxes, or temperature dependent paleo-microbial abundances remain unquantified as to their significance (if any). These paleo-effects on weathering and erosion rates warrant future investigation.

Second, there are several methodological aspects of this study that warrant mentioning. In all the Chilean and global data compilations presented a replicate analysis at each sample location is not available. For the Chilean data (and often times in

many of the global studies referenced) the common practice is to collect an amalgamated sample across an exposed horizon (often times ~1 m wide, the width of the pedon) for analysis. Due to the considerable effort involved in excavating pedons, rarely is a replicate analysis conducted in these types of geochemical studies. The implication is that analysis of results with replicate sample locations reduces the types of statistical analyses that can be done to understand how representative the sample location is. In this study we compared observed soil production, chemical weathering, and physical erosion rates to globally derived data sets for topography, and climate (See Supplementary Material S1). This approach ensures that all data are treated consistently, but does not evaluate how representative these global compilations are to more regional data sets. For example, the CHELSA climate data set used here is a downscaled (to ~900 m) product derived from the ERA-interim reanalysis data. The ERA-interim data is widely used in the climate sciences and is derived from ground, ocean, and satellite meteorological observations. However, more regional reanalysis data products exist for some of the study areas covered in our global compilation that might capture orographic effects in precipitation better than a 900 m resolution global product. However, such regional downscale products are not available in many places (globally) and there are diverse techniques applied for downscaling climate data. Furthermore, not all regional climate data is peer-reviewed. Given this, a mixing and matching of different regional climate products (produced via different techniques) versus using global data products (produced with a consistent downscaling approach everywhere) would lead to its own, technique based, uncertainties and biases. Given these types of complications, we have restricted our analysis to global data products produced with a consistent set of techniques, but acknowledge that future global data products conducted at higher resolution may provide an improved analysis to build upon the results presented here.

6 Conclusion

Soil production, chemical weathering, and physical erosion rates change under the climate and vegetation gradients in the Chilean Coastal Cordillera. Whereas vegetation cover and mean annual precipitation increase from north to south, mean annual temperature decreases. SPRs increase from Pan de Azúcar to La Campana and decrease slightly, or possible stay the same, in Nahuelbuta. Chemical weathering rates increase from zero in the north to a maximum of of 211 t/(km^2 yr) in La Campana. Physical erosion rates are low in Pan de Azúcar (~10 t/(km^2 yr)), increase towards the south and are highest in La Campana. Combined total chemical weathering and physical erosion rates indicate that the total denudation rates are lowest in Pan de Azúcar and highest in La Campana. The contribution of chemical weathering to the total denudation rate is negligible in the north, and increases to ~50% towards the south, and is lower again in Nahuelbuta. The observations made in the Chilean Coastal Cordillera and our comparison to global data lead to the following conclusions for the hypotheses stated in section 1.0:

1) Calculated soil production as well as chemical weathering rates do not increase monotonically with increasing mean annual precipitation. The decrease in SPRs at higher precipitation and vegetation cover is likely due to thicker and more nutrient depleted soils in settings with higher vegetation/LAI causing vegetation to switch to a nutrient recycling mode of near surface material (e.g., Jobbágy and Jackson, 2001) rather than harvesting fresh nutrients from deeply buried bedrock that would

facilitate continued soil production. Thus, vegetation cover could be providing the 'biotic break' responsible for this speed limit. The observed decrease in chemical weathering rates is also at odds with an increasing chemical index of alteration, which indicates an increase in the weathering trend from north to south. One explanation for the calculated low chemical weathering rate in the southernmost study area is the mobile behavior of generally immobile elements under high precipitation rates. Another explanation could be the protective nature of thick and clay-rich soils to intense weathering in the saprolite. Finally, latitudinal variations in microbial abundance due to climate and soil pH variations may influence biotically driven chemical weathering rates.

2) Calculated physical erosion rates increase and then stabilize from north to south with increasing precipitation. This stabilization may be caused by increasing vegetation cover protecting the soil from physical erosion.

3) The contribution of chemical weathering to total denudation rates increases and then decreases from north to south. In the northernmost study area, the low contribution in chemical weathering to total denudation is due to the lack of a weathering agent. In contrast, in the southernmost study area, where solute fluxes are high and soil and saprolite are rich in organic acids, thick soils and/or clay minerals may protect saprolite from intense chemical weathering.

To conclude, soil production, chemical weathering, and physical erosion rates change with increasing MAP and LAI non-linearly and non-monotonically. Whereas increasing MAP has the potential to increase chemical weathering and physical erosion rates, vegetation decreases physical erosion rates and to a certain extent also chemical weathering rates.

Author contribution

Both authors (MS, TAE) contributed equally to the planning, execution, and manuscript preparation.

Competing interest

The authors declare that they have no conflict of interest.

Acknowledgement

We would like to thank the Chilean National Forestry Corporation (CONAF) for providing access to the sample locations and on-site support of our research. Furthermore we would like to thank to anonymous reviewers for their insightful comments.

Financial support

This work was funded by the German Science Foundation (DFG) priority research program SPP-1803 "EarthShape: Earth Surface Shaping by Biota" (grant SCHA 1690/3-1 to MS and EH329/14-2 to TAE).

References

Amundson, R., Heimsath, A., Owen, J., Yoo, K. and Dietrich, W. E.: Hillslope soils and vegetation, Geomorphology, 234, 122–132, doi:10.1016/j.geomorph.2014.12.031, 2015.

Bahram, M., Hildebrand, F., Forslund, S.K., Anderson, J.S., Soudzilovskaia, N.A., Bodegom, P.M., Bengtsson-Palme, J., Anslan, S., Coelho, L.P., Harend, H., Huerta-Cepas, J., Medema, M.H., Maltz, M.R., Mundra, S., Olsson, P.A., Pent, M., Põlme, S., Sunagawa, S., Ryberg, M., Tedersoo, L. and Bork, P.: Structure and function of the global topsoil microbiome, Nature, 560, 233-237, doi.org/10.1038/s41586-018-0386-6, 2018.

Bernhard, N., Moskwa, L.-M., Schmidt, K., Oeser, R. A., Aburto, F., Bader, M. Y., Baumann, K., von Blanckenburg, F., Boy, J., van den Brink, L., Brucker, E., Büdel, B., Canessa, R., Dippold, M. A., Ehlers, T. A., Fuentes, J. P., Godoy, R., Jung, P., Karsten, U., Köster, M., Kuzyakov, Y., Leinweber, P., Neidhardt, H., Matus, F., Mueller, C. W., Oelmann, Y., Oses, R., Osses, P., Paulino, L., Samolov, E., Schaller, M., Schmid, M., Spielvogel, S., Spohn, M., Stock, S., Stroncik, N., Tielbörger, K., Übernickel, K., Scholten, T., Seguel, O., Wagner, D. and Kühn, P.: Pedogenic and microbial interrelations to regional climate and local topography: New insights from a climate gradient (arid to humid) along the Coastal Cordillera of Chile, CATENA, 170, 335–355, doi:10.1016/j.catena.2018.06.018, 2018.

Binnie, S.A., Phillips, W.M., Summerfield, M.A., Fifield, L.K.: Tectonic uplift, threshold hillslopes, and denudation rates in a developing mountain range, Geology, 35, 743-746, doi: 10.1130/G23641A.1, 2007.

Borchers, B., Marrero, S., Balco, G., Caffee, M., Goehring, B., Lifton, N., Nishiizumi, K., Phillips, F., Schaefer, J. and Stone, J.: Geological calibration of spallation production rates in the CRONUS-Earth project, Quaternary Geochronology, 31, 188–198, doi:10.1016/j.quageo.2015.01.009, 2016.

Braucher, R., Merchel, S., Borgomano, J. and Bourlès, D. L.: Production of cosmogenic radionuclides at great depth: A multi element approach, Earth and Planetary Science Letters, 309(1–2), 1–9, doi:10.1016/j.epsl.2011.06.036, 2011.

Burke, B.C., Heimsath, A.M. and White, A.F.: Coupling chemical weathering with soil production across soil-mantled landscapes, Earth Surf. Process. Landforms, 32(6), 853–873, doi:10.1002/esp.1443, 2007.

Buss, H.L., Bruns, M.A., Schultz, M.J., Moore, J., Mathur, C.F. and Brantley, S.L.: The coupling of biological iron cycling and mineral weathering during saprolite formation, Luquillo Mountains, Puerto Rico, Geobiology, 3, 247-260, doi.org/10.1111/j.1472-4669.2006.00058.x, 2005.

Dixon, J.L., Heimsath, A.M. and Amundson, R.: The critical role of climate and saprolite weathering in landscape evolution, Earth Surf. Process. Landforms, 34(11), 1507–1521, doi:10.1002/esp.1836, 2009.

Dixon, J.L. and von Blanckenburg, F.: Soils as pacemakers and limiters of global silicate weathering, Comptes Rendus Geoscience, 344(11–12), 597–609, doi:10.1016/j.crte.2012.10.012, 2012.

Eilers, K.C., Debenport, S., Anderson, S. and Fierer N.: Digging deeper to find unique microbial communities: The strong effect of depth on the structure of bacterial land archaeal communities in soil, Soil Biology and Biochemistry, 50, 58-65, doi:10.1016/j.soilbio.2012.03.011, 2012.

Ferrier, K.L., Kirchner, J.W. and Finkel, R.C.: Weak influences of climate and mineral supply rates on chemical erosion rates: Measurements along two altitudinal transects in the Idaho Batholith: CLIMATE AND CHEMICAL EROSION RATES, J. Geophys. Res., 117(F2), n/a-n/a, doi:10.1029/2011JF002231, 2012.

Fierer, N. and Jackson, R.B.: The diversity and biogeography of soil bacterial communities, PNAS, 103 (3), 626-631, doi:10.1073/pnas.0507535103, 2006.

Granger, D.E. and Riebe, C.S.: Cosmogenic Nuclides in Weathering and Erosion, in Treatise on Geochemistry, pp. 401–436, Elsevier., 2014.

Heimsath, A.M. and Whipple, K.X.: Strength matters: Resisting erosion across upland landscapes, Earth Surf. Process. Landforms, 44(9), 1748–1754, doi:10.1002/esp.4609, 2019.

Heimsath, A.M., Dietrich, W.E., Nishiizumi, K. and Finkel, R.C.: The soil production function and landscape equilibrium, Nature, 388(6640), 358–361, doi:10.1038/41056, 1997.

Heimsath, A.M., Furbish, D.J. and Dietrich, W.E.: The illusion of diffusion: Field evidence for depth-dependent sediment transport, Geol, 33(12), 949, doi:10.1130/G21868.1, 2005.

Heimsath, A.M., DiBiase, R.A. and Whipple, K.X.: Soil production limits and the transition to bedrock-dominated landscapes, Nature Geosci, 5(3), 210–214, doi:10.1038/ngeo1380, 2012.

IUSS Working Group WRB. World reference base for soil resources 2014, update 2015. Prepared by Schad P, van Huyssteen C, Micheli E. 192 pp. World Soil Resources Reports No. 106, FAO, Rome. 2015.

Jobbágy, E.G. and Jackson, R.B.: The distribution of soil nutrients with depth: global patterns and the imprint of plants, Biogeochemistry, 53, 51-77, 2001.

Karger, D.N., Conrad, O., Böhner, J., Kawohl, T., Kreft, H., Soria-Auza, R.W., Zimmermann, N.E., Linder, H.P. and Kessler, M.: Climatologies at high resolution for the earth's land surface areas, Scientific Data, 4, sdata2017122, doi:10.1038/sdata.2017.122, 2017.

Koester, M., Stock, S.C., Nájera, F., Abdallah, K., Gorbushina, A., Prietzel, J., Matus, F., Klysubun, W., Boy, J., Kuzyakov, Y., Dippold, M.A., Spielvogel, S.: From rock eating to vegetarian ecosystems - Disentangling processes of phosphorus acquisition across biomes, Geoderma, doi.org/10.1016/j.geoderma.2020.114827, 2020.

Langbein, W.B. and Schumm, S.A.: Yield of sediment in relation to mean annual precipitation, Transactions, American Geophysical Union, 39, 1076–1084, doi:10.1029/TR039i006p01076, 1958.

Larsen, I.J., Almond, P.C., Eger, A., Stone, J.O., Montgomery, D.R. and Malcolm, B.: Rapid Soil Production and Weathering in the Southern Alps, New Zealand, Science, 343(6171), 637–640, doi:10.1126/science.1244908, 2014.

Lebedeva, M.I. and Brantley, S.L.: Exploring an 'ideal hill': how lithology and transport mechanisms affect the possibility of a steady state during weathering and erosion, Earth Surface Processes and Landforms, 45, 625-665, doi: 10.1002/esp.4762, 2020.

Marrero, S.M., Phillips, F.M., Borchers, B., Lifton, N., Aumer, R. and Balco, G.: Cosmogenic nuclide systematics and the CRONUScalc program, Quaternary Geochronology, 31, 160–187, doi:10.1016/j.quageo.2015.09.005, 2016.

Mishra, A.K., Placzek, C. and Jones, R.: Coupled influence of precipitation and vegetation on millennial-scale erosion rates derived from 10Be, edited by A. Zerboni, PLoS ONE, 14(1), e0211325, doi:10.1371/journal.pone.0211325, 2019.

Mutz, S.G., Ehlers, T.A., Werner, M., Lohmann, G., Stepanek, C. and Li, J.: Estimates of late Cenozoic climate change relevant to Earth surface processes in tectonically active orogens, Earth Surface Dynamics, 6, 271–301, doi:10.5194/esurf-6-271-2018, 2018.

Mutz, S.G., Ehlers, T.A.: Detection and explation of spatiotemporal patterns in Late Cenozoic paleoclimate change relevant to Earth surface proceses, Earth Surface Dynamics, 7, 663–679, doi.org/10.5194/esurf-7-663-2019, 2019.

Nesbitt, W. and Young, G.M.: Early Proterozoic climates and plate motions inferred from major element chemistry of lutites, Nature, 299, 715-717, 1982.

Norton, K.P. and von Blanckenburg, F.: Silicate weathering of soil-mantled slopes in an active Alpine landscape, Geochimica et Cosmochimica Acta, 74(18), 5243–5258, doi:10.1016/j.gca.2010.06.019, 2010.

Norton, K.P., Molnar, P. and Schlunegger, F.: The role of climate-driven chemical weathering on soil production, Geomorphology, 204, 510–517, doi:10.1016/j.geomorph.2013.08.030, 2014.

Oeser, R.A., Stroncik, N., Moskwa, L.-M., Bernhard, N., Schaller, M., Canessa, R., van den Brink, L., Köster, M., Brucker, E., Stock, S., Fuentes, J.P., Godoy, R., Matus, F.J., Oses Pedraza, R., Osses McIntyre, P., Paulino, L., Seguel, O., Bader, M. Y., Boy, J., Dippold, M.A., Ehlers, T.A., Kühn, P., Kuzyakov, Y., Leinweber, P., Scholten, T., Spielvogel, S., Spohn, M., Übernickel, K., Tielbörger, K., Wagner, D. and von Blanckenburg, F.: Chemistry and microbiology of the Critical Zone along a steep climate and vegetation gradient in the Chilean Coastal Cordillera, CATENA, 170, 183–203, doi:10.1016/j.catena.2018.06.002, 2018.

Oeser, R.A. von Blanckenburg F.: Do degree and rate of silicate weathering depend on plant productivity? Biogeosciences. https://doi.org/10.5194/bg-17-4883-2020, 2020.

Peay, K.G., von Sperber, C., Candarelli, E., Toju, H., Francis, C.A., Chadwick, O.A. and Vitousek, P.M., Convergence and contrast in the community structure of Bacteria, Fungi and Archaea along a tropical elevation-climate gradient, FENS Microbiology Ecology, 93, doi: 10.1093/gemsec/fix0045, 2017/

Pelak, N.F., Parolari, A.J. and Porporato, A.: Bistable plant-soil dynamics and biogenic controls on the soil production function: BISTABLE PLANT-SOIL DYNAMICS, Earth Surf. Process. Landforms, 41(8), 1011–1017, doi:10.1002/esp.3878, 2016.

Pelletier, J.D. and Rasmussen, C.: Quantifying the climatic and tectonic controls on hillslope steepness and erosion rate, Lithosphere, 1(2), 73–80, doi:10.1130/L3.1, 2009.

Perron, J.T.: Climate and the pace of erosional landscape evolution, Annual Review of Earth and Planetary Sciences, 45, 461-491, doi.org/10.1146/annurev- earth- 060614- 105405, 2017

Plug, L.J., Gosse, J.C., McIntosh, J.J. and Bigley, R.: Attenuation of cosmic ray flux in temperate forest, J. Geophys. Res., 112(F2), F02022, doi:10.1029/2006JF000668, 2007.

Rasmussen, C. and Tabor, N.J.: Applying a Quantitative Pedogenic Energy Model across a Range of Environmental Gradients, Soil Science Society of America Journal, 71(6), 1719, doi:10.2136/sssaj2007.0051, 2007.

Richardson, P.W., Perron, J.T. and Schurr, N.D.: Influences of climate and life on hillslope sediment transport, Geology, 47(5), 423–426, doi:10.1130/G45305.1, 2019.

Riebe, C.S. and Granger, D.E.: Quantifying effects of deep and near-surface chemical erosion on cosmogenic nuclides in soils, saprolite, and sediment: EFFECTS OF CHEMICAL EROSION ON COSMOGENIC NUCLIDE BUILDUP, Earth Surf. Process. Landforms, 38(5), 523–533, doi:10.1002/esp.3339, 2013.

Riebe, C.S., Kirchner, J.W., Granger, D.E. and Finkel, R.C.: Strong tectonic and weak climatic control of long-term chemical weathering rates, Geology, 29, 511-514, 2001.

Riebe, C.S., Kirchner, J.W. and Finkel, R.C.: Erosional and climatic effects on long-term chemical weathering rates in granitic landscapes spanning diverse climate regimes, Earth and Planetary Science Letters, 224(3–4), 547–562, doi:10.1016/j.epsl.2004.05.019, 2004a.

Riebe, C.S., Kirchner, J.W. and Finkel, R.C.: Sharp decrease in long-term chemical weathering rates along an altitudinal transect, Earth and Planetary Science Letters, 218(3–4), 421–434, doi:10.1016/S0012-821X(03)00673-3, 2004b.

Schaller, M., Ehlers, T.A., Lang, K.A.H., Schmid, M. and Fuentes-Espoz, J.P.: Addressing the contribution of climate and vegetation cover on hillslope denudation, Chilean Coastal Cordillera (26°–38°S), Earth and Planetary Science Letters, 489, 111–122, doi:10.1016/j.epsl.2018.02.026, 2018.

Schmid, M., Ehlers, T.A., Werner, C., Hickler, T., and Fuentes-Espoz, J.-P. Effect of changing vegetation and precipitation on denudation – Part 2: Predicted landscape response to transient climate and vegetation cover over millennial to million-year timescales, Earth Surface Dynamics, 6(4), 859–881, doi:10.5194/esurf-6-859-2018, 2018.

Starke, J., Ehlers, T.A. and Schaller, M.: Latitudinal effect of vegetation on erosion rates identified along western South America, Science, 367(6484), 1358–1361, https://doi.org/10.1126/science.aaz0840, 2020.

Taboada, T., Cortizas, A.M., García, C. and García-Rodeja, E.: Particle-size fractionation of titanium and zirconium during weathering and pedogenesis of granitic rocks in NW Spain, Geoderma, 131(1–2), 218–236, doi:10.1016/j.geoderma.2005.03.025, 2006.

Tan, W., Wang, J., Bai, W., Qi, J. and Chen, W.: Soil bacterial diversity correlates with precipitation and soil pH in long-term maize cropping systems, Scientific Reports, 10, 6012, doi.org/10.1038/s41598-020-62919-7, 2020.

Werner, C., Schmid, M., Ehlers, T.A., Fuentes-Espoz, J.P., Steinkamp, J., Forrest, M., Liakka, J., Maldonado, A. and Hickler, T.: Effect of changing vegetation and precipitation on denudation – Part 1: Predicted vegetation composition and cover over the last 21 thousand years along the Coastal Cordillera of Chile, Earth Surface Dynamics, 6, 829–858, doi:10.5194/esurf-6-829-2018, 2018.

Yoo, K., Amundson, R., Heimsath, A.M., Dietrich, W.E. and Brimhall, G.H.: Integration of geochemical mass balance with sediment transport to calculate rates of soil chemical weathering and transport on hillslopes, Journal of Geophysical Research, 112(F2), doi:10.1029/2005JF000402, 2007.

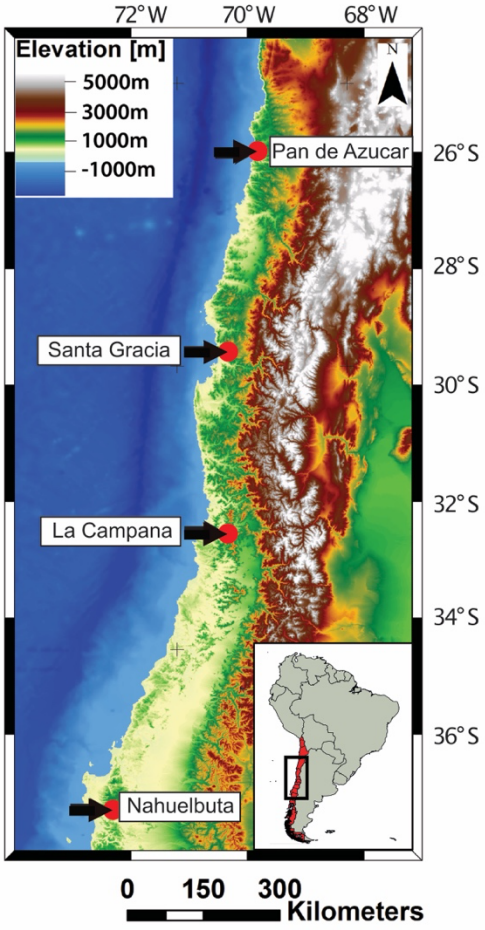

720 **Figure 1: Digital elevation model (Data source: GTOPO30) with the locations of the four study areas (red circles) in the Chilean Coastal Cordillera. The climate from north to south over ~1200 km changes from arid to temperate humid. See Supplementary Material figure S1 photographs of each area and detailed satellite images of sample locations.**

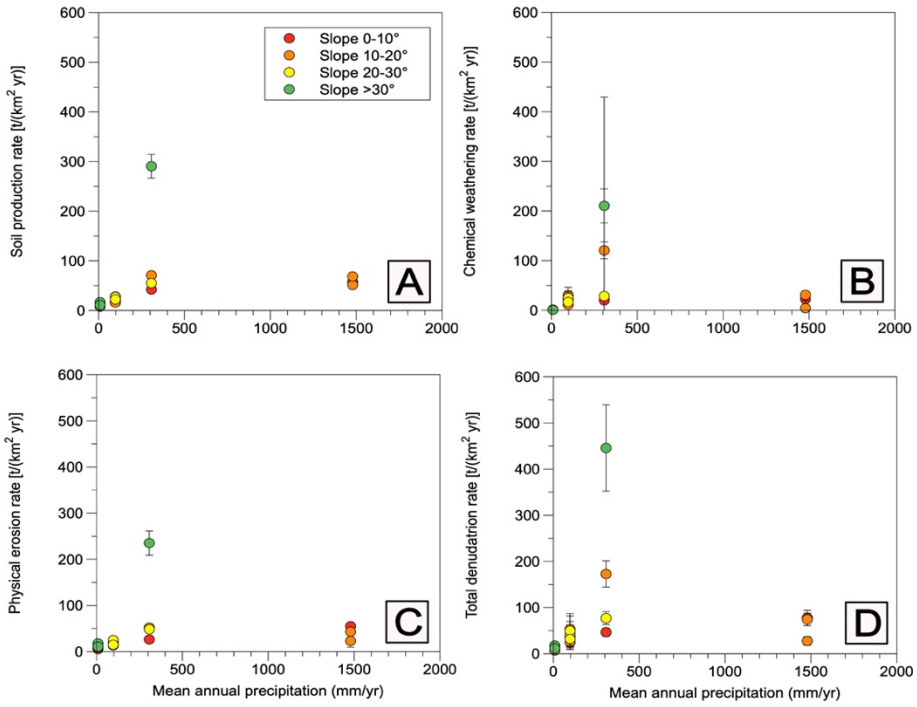

Figure 2: Cosmogenic nuclide-derived rates from pedon locations for four study areas in the climate and vegetation gradient of the Chilean Coastal Cordillera (From north to south and with increasing mean annual precipitation: Pan de Azúcar, Santa Gracia, La Campana, and Nahuelbuta): A) Soil production rates, B) chemical weathering rates, C) physical erosion rates, and D) total denudation rates versus mean annual precipitation

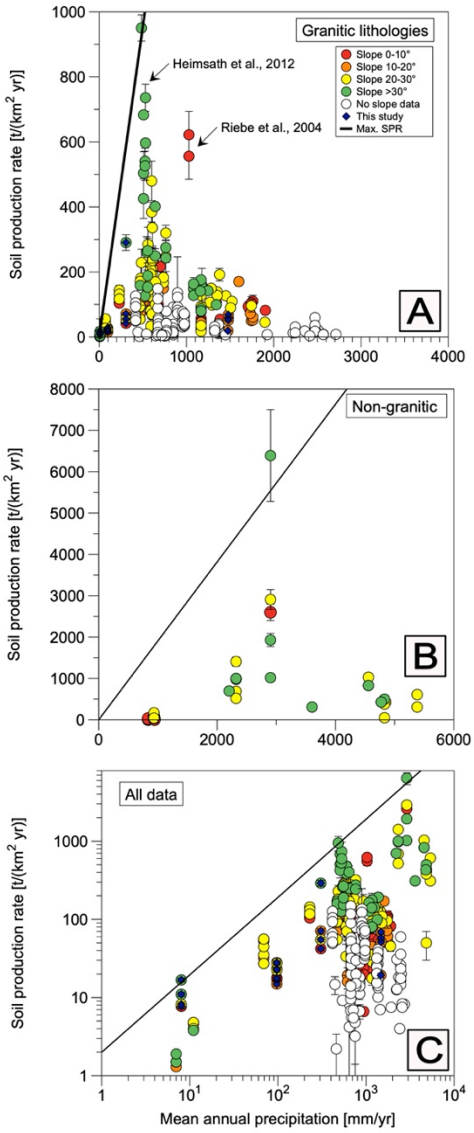

Figure 3: Soil production rates SPRs versus mean annual precipitation: A) SPRs from granitic lithologies such as samples from this study (blue diamonds). The data are in bins for different slopes. Note the linear axes as well as the black line for the maximum production rate after Norton et al. (2014) at a temperature of 14ºC. B) SPRs from some non-granitic lithologies. Note the increased linear axis in comparison to Fig. 3A. C) Compilation of all SPRs plotted with logarithmic axis.

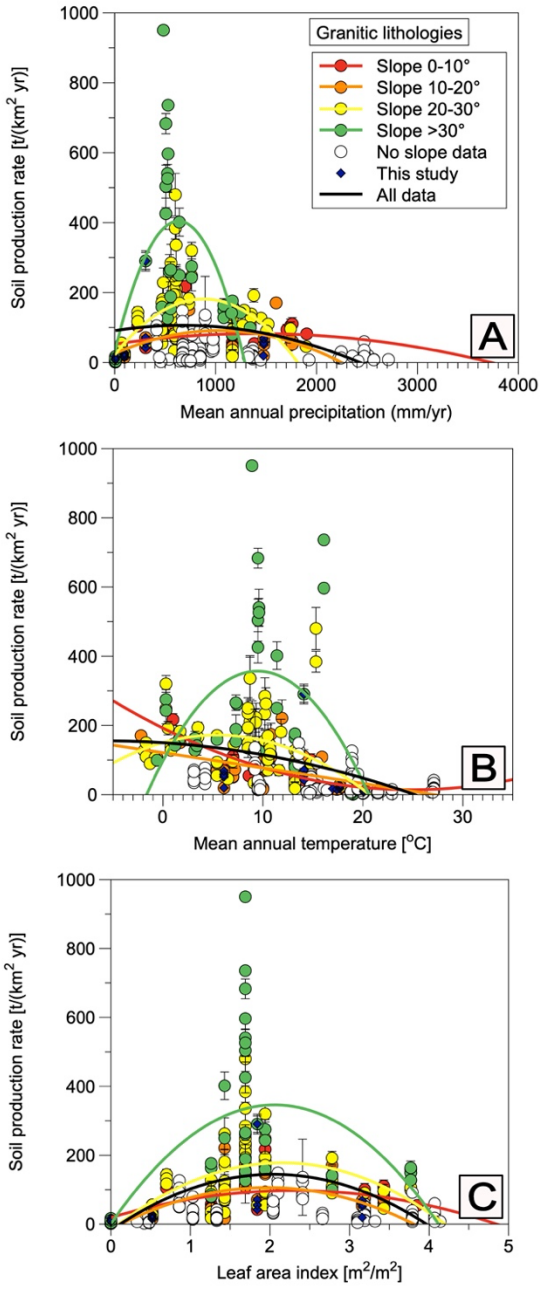

735 **Figure 4: Soil production rates from this study (blue diamonds) and other studies in hillslopes with granitic lithologies versus: A) Mean annual precipitation, B) Mean annual temperature, and C) Leaf area index. Data are separated in slope bins and plotted with a binomial fit.**

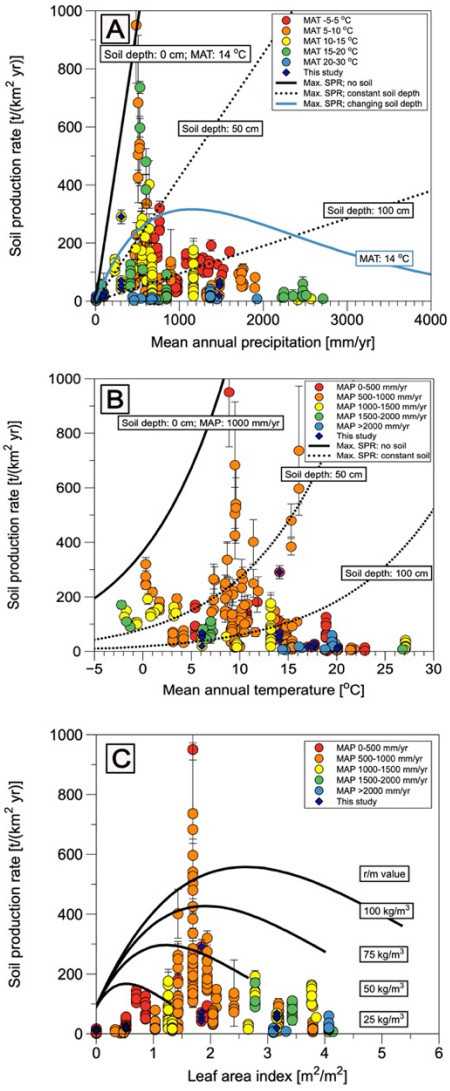

740 **Figure 5: Soil production rates versus: A) Mean annual precipitation. The black bold and stippled lines indicate maximum SPRs for different soil depths (after Norton et al., 2014). The blue line is the maximum SPR with increasing soil depth with increasing mean annual precipitation. Data are sorted in mean annual temperature bins. B) Mean annual temperature. Black and stippled lines are maximum SPRs for different soil depths. Data sorted in mean annual precipitation bins. C) Leaf area index. Black lines are maximum SPRs for different biomasses (r/m value; after Pelak et al., 2016). Data sorted in mean annual precipitation bins.**

745

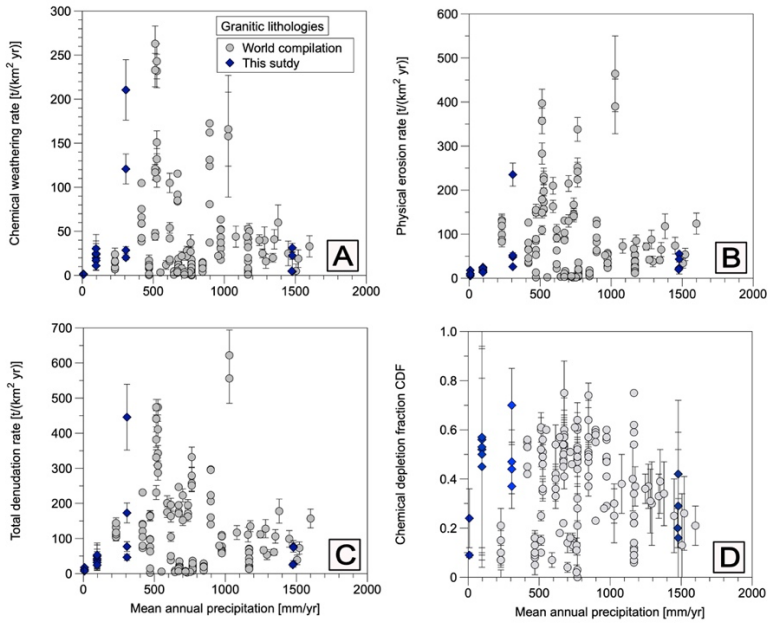

Figure 6: A) Chemical weathering rates, B) Physical erosion rates, C) Denudation rate, and D) Chemical depletion fraction CDF versus mean annual precipitation. Rates for the four study areas (blue diamonds) and comparison rates from different study areas situated in granitic soil-mantled hillslopes (gray dots).

750